Direct-to-Earth Communications with Mars Science Laboratory during Entry, Descent, and Landing

Melissa Soriano, Susan Finley, David Fort, Brian Schratz, Peter Ilott,
Ryan Mukai, Polly Estabrook, Kamal Oudrhiri, Daniel Kahan, Edgar Satorius
Jet Propulsion Laboratory
California Institute of Technology
Pasadena, CA 91109
818-393-7632
Melissa.A.Soriano@jpl.nasa.gov

***Abstract*— Mars Science Laboratory (MSL) undergoes extreme heating and acceleration during Entry, Descent, and Landing (EDL) on Mars. Unknown dynamics lead to large Doppler shifts, making communication challenging. During EDL, a special form of Multiple Frequency Shift Keying (MFSK) communication is used for Direct-To-Earth (DTE) communication. The X-band signal is received by the Deep Space Network (DSN) at the Canberra Deep Space Communication complex, then down-converted, digitized, and recorded by open-loop Radio Science Receivers (RSR), and decoded in real-time by the EDL Data Analysis (EDA) System. The EDA uses lock states with configurable Fast Fourier Transforms to acquire and track the signal. RSR configuration and channel allocation is shown. Testing prior to EDL is discussed including software simulations, test bed runs with MSL flight hardware, and the in-flight end-to-end test. EDA configuration parameters and signal dynamics during pre-entry, entry, and parachute deployment are analyzed. RSR and EDA performance during MSL EDL is evaluated, including performance using a single 70-meter DSN antenna and an array of two 34-meter DSN antennas as a back up to the 70-meter antenna.**

TABLE OF CONTENTS

1. INTRODUCTION 1
2. APPROACH 2
3. DETAILED ANALYSIS 3
4. RESULTS.....9
5. CONCLUSION.....11
6. ACKNOWLEDGEMENTS.....11
REFERENCES.....12

1. INTRODUCTION

During Mars Science Laboratory (MSL)'s Entry, Descent, and Landing (EDL), there were two forms of real-time communication: Direct-to-Earth (DTE) and relay through Mars Odyssey orbiter. DTE communication was transmitted by MSL's Small Deep Space Transponder (SDST) at X-band frequencies and received at the Canberra Deep Space Communications Complex (CDSCC) in Australia.

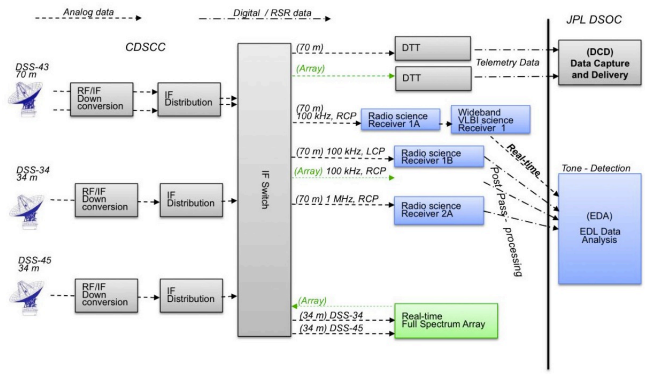

Figure 1- MSL EDL Direct-To-Earth Communications system diagram

A DTE Communications system diagram is shown in Figure **1**. Three antennas at CDSCC received the DTE signal: DSS-43 (70-m), DSS-34 (34-m), and DSS-45 (34-m), with DSS-43 being prime. Both Right Circular Polarization (RCP) and Left Circular Polarization (LCP) signals were received and down-converted to Intermediate Frequency (IF) and recorded from DSS-43, as well as RCP signals from DSS-34 and DSS-45. MSL's transmitted signal was RCP. The signals from DSS-34 and DSS-45 were also correlated and combined by the Full Spectrum Processor Array (FSPA) and recorded as a back up to DSS-43.

Analog data from the antennas were distributed to closed-loop Downlink Telemetry, and Tracking (DTT) receivers, the FSPA, and open-loop Radio Science Receivers (RSR). During EDL, traditional phase modulated low rate telemetry is not possible due to high dynamics and low signal-to-noise ratio. The closed-loop DTT receivers received the signal on a best-efforts basis but as expected, did not stay locked through banking and parachute deployment. The open-loop RSRs were prime for EDL. The RSRs digitized, filtered, and down-converted the signal, using a 100 kHz 8-bit complex channel. This data was relayed to the Wideband VLBI Science Receiver (WVSR) and transferred across the flight operations network from CDSCC in Australia to the EDL Data Analysis (EDA) assemblies at JPL's Deep Space Operations Complex (DSOC).

978-1-4673-1813-6/13/$31.00 ©2013 IEEE

The EDAs processed the 70-m data using Fast Fourier Transform (FFT) based algorithms in real-time using acquisition and tracking lock states [4]. Each lock state may have different FFT parameters such as length of integration. Up to three threads and twelve processors work in parallel. The signal has a carrier and a subcarrier (or tone). The received EDL signal, *s(t)*, is shown in the equation below, where f_c is the transmitted carrier frequency, f_d is the data tone frequency, Δ is the modulation index, and P_t is the total received power.

$$s(t) = \sqrt{2P_t}\cos\left\{2\pi\int_{-\infty}^{t} d\tau \cdot f_c(\tau) + \Delta \cdot Sqr\left(2\pi\int_{-\infty}^{t} d\tau \cdot f_d(\tau)\right)\right\} + n(t) \quad (1)$$

where $Sqr(x)$ is the hard-limited sine function:

$$Sqr(x) = \begin{cases} 1, & 0 < x \leq \pi \\ -1, & \pi < x \leq 2\pi \end{cases} \quad (2)$$

The subcarrier's offset from the carrier varies and this difference conveys a meaning. An example FFT spectrum for *s(t)* with Δ = 43° is shown in Figure **2**. The EDA searches for the carrier and data tone using peak power detection and then measures the difference between the carrier and subcarrier, which is converted to a tone mnemonic. During MSL EDL, tone mnemonics as well as plots of residual frequency and signal-to-power ratio were provided in real-time to the Mission Support Area.

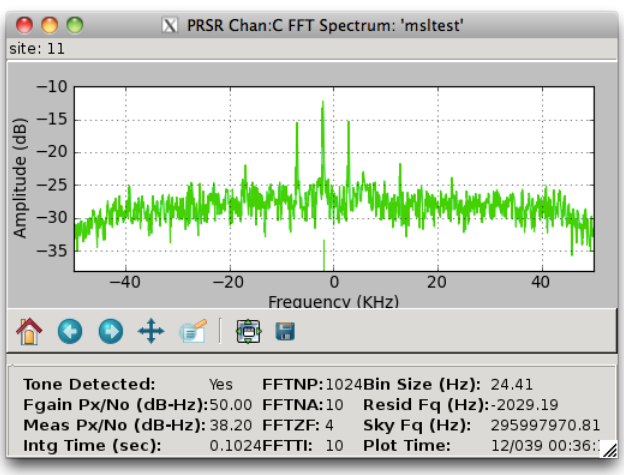

Figure 2- FFT of MSL EDL signal

For MER and Juno, Δ = 48°. The received carrier and data powers are functions of P_t and Δ. As shown by the below equations, the choice of modulation index is a tradeoff between power in the carrier, P_c, for acquisition/tracking and power in the data, P_d, for tone detection. Note that P_d includes the power in the first tone harmonic, denoted by P_{tone}, and also the power in the other harmonics. The ratio of P_d to P_{tone} is 1.2337 [1]. MSL's selection of Δ = 48° vs Δ = 43° for MER and Juno puts less of the total transmitted power in the carrier.

$$P_c = P_t \cdot cos^2\Delta \quad (3)$$

$$P_d = P_t \cdot sin^2\Delta \quad (4)$$

$$P_{tone} = \frac{P_t \cdot sin^2\Delta}{1.2337} \quad (5)$$

2. Approach

The DTE Communications system was tested in an in-flight test, with a Portable Radio Science Receiver (PRSR) and the MSL test bed, and using software simulations of expected Doppler dynamics.

In-Flight Test

An in-flight test of the DTE communications system planned for MSL EDL took place on DOY 179, 2012. This test included two main parts: a. All 256 tones were tested with 10-second durations, ramping up from tone 1 to tone 256 and then ramping back down to tone 1. Tone number vs time (in seconds) for this part of the test is shown in Figure **3**. b. An abbreviated version of the nominal EDL sequence was also tested. Tone number vs time for this part of the test is shown in Figure **4**. Note the heartbeat tones (which are played if there is no other event taking place) at tone numbers 233 and 239. The in-flight test was successful and all radiated tones were correctly detected.

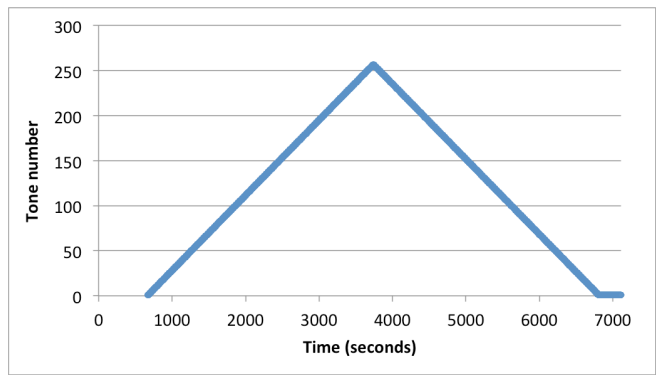

Figure 3- Tone number vs Time (seconds) for in-flight test, tones ramp

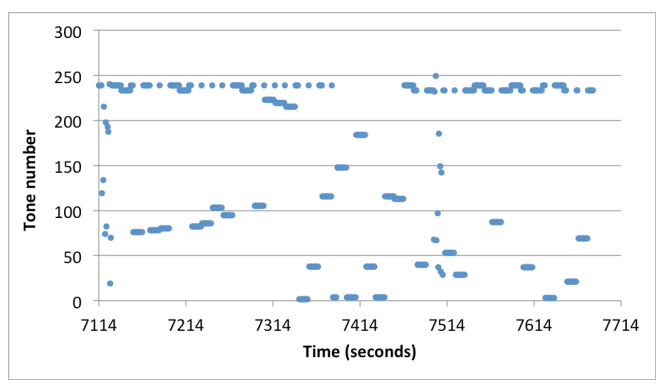

Figure 4- Tone number vs Time (seconds) for in-flight test, nominal EDL

Software simulations

Simulated signals were generated in the standard Radio Science Receiver (RSR) file format and processed by the Entry, Decent, and Landing (EDL) Data Analysis (EDA) system. These data files were generated using eda/gen, which is part of the EDA software package. The eda/gen software accepts as input a file in standard downlink frequency predicts format. Residual frequency is computed by differencing the measured signal frequency and the predicted frequency.

$$f_{residual} = f_{measured} - f_{predicts} \tag{6}$$

For the spacecraft predicts, a downlink frequency predicts file was provided by Dan Burkhart of MSL Navigation. In this file, parachute deployment and powered descent do not occur; the spacecraft impacts at around E+300 s. A discontinuity occurs at this point, as seen in Figure **5**. The lack of parachute deployment in the predicts file is deliberate and desirable because the exact time of parachute deployment is unknown. If parachute deployment were included, residual frequency would spike twice, at the predicted time and actual time. With parachute deployment removed from the predicts, the spike in residual frequency occurs only at the actual time and is more easily detected in real-time. The spacecraft predicts file has an entry time at MSL of 06-AUG-2012 05:10:43.8725 UTC. Distance from MSL to CDSCC at this entry time resulted in a one-way light time (OWLT) of 827.226 seconds. Entry time at Earth is, therefore, 06-AUG-2012 05:24:31.9465 UTC.

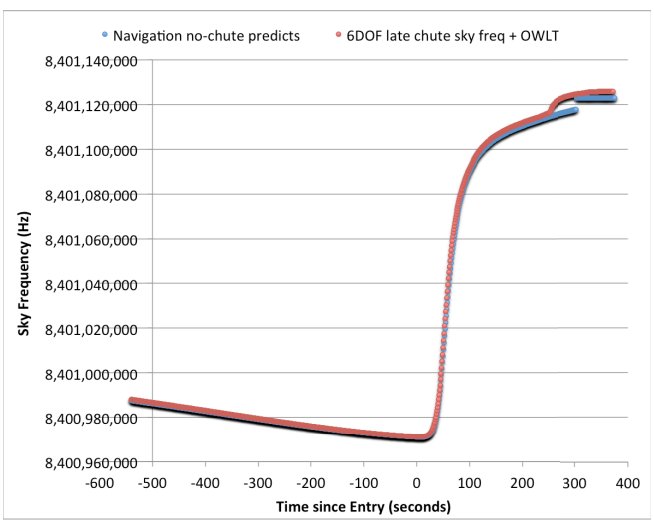

Figure 5- 6DOF late chute signal and Navigation no-chute predicts

For the measured signal, data from the 6 Degrees of Freedom (6DOF) model provided by Jeremy Schidner of NASA Langley were used. Data for the latest, earliest, and nominal times of parachute deployment were obtained and this data is shown in Figure **6**. We will call this data "late," "early," and "nominal" respectively. The 6DOF late chute signal and navigation predicts are shown in Figure **5**.

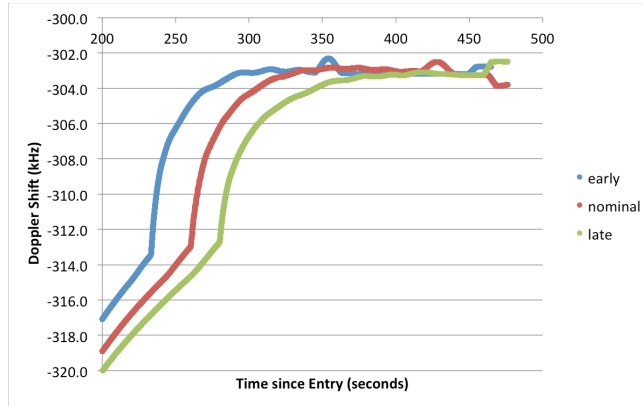

Figure 6- Overview of 6DOF parachute cases

Residual frequency was computed by differencing these early and late bounding cases for the spacecraft signal and the downlink frequency predicts provided by MSL navigation. Software simulations were generated using these frequency residuals and used to test the EDA parameters [6]. Similar work was done prior to MSL's launch in which simulated signals were also generated in RSR file format and processed by the operational EDA software for Mars Science Laboratory. This work demonstrated 97% correct tones detection at total received signal power (carrier plus data)-to-noise density ratio (P_t/N_o) of 20 dB-Hz, 79-81% detection at 18 dB-Hz, and 16% detection at 16 dB-Hz [2].

MSL Test Bed

In addition to simulations, the EDA was tested in over 25 runs with MSL test bed. In preparation for EDL, the engineering model of the flight hardware and software was tested numerous times, including the Telecom system. The Intermediate Frequency (IF) signal was converted from analog to fiber optic, travelled across the lab via a fiber-optic link, was then converted back to analog, and fed as input to a PRSR. The PRSR digitized, down-converted, filtered, and recorded the signal. The data was then streamed in real-time to the EDA. However, the standard test bed runs did not include Doppler dynamics. Robustness tests combined the signal from MSL test bed with new navigation predicts that included Doppler dynamics from the 6DOF data.

3. Detailed Analysis

Theoretical Probability of Detection

Searching for the signal amid frequency and frequency rate bins entails finding the bin with the largest squared value. Assuming the noise to be zero-mean Gaussian, each bin will have a chi-squared distribution. The bin containing the signal will have a non-central chi-squared distribution [1].

Let the probability density function (PDF) of the signal be denoted by $f_s(x)$, and let the cumulative distribution function (CDF) of the noise bins be denoted by $F_n(x)$. Let

N_f be the total number of bins to be searched. The probability of correct detection is given by:

$$\int_{x=0}^{x=+\infty} f_s(x)[F_n(x)]^{N_f-1}dx \tag{7}$$

The expression above is the probability that each noise bin has a value lower than that of the signal bin. We provide both the PDF of the signal bin and the CDF of the noise bins next. These are defined in terms of several other terms listed below:

1. N_{FFT}: Number of points per FFT. This is the number of frequency bins over which we must search for the residual carrier.
2. Δf: Frequency resolution. This is the sampling rate (100 kHz in this case) divided by N_{FFT}. The result is the frequency resolution of the FFT.
3. T: The time of incoherent integration.
4. $CNR\ or\ \frac{P_c}{N_0}$: This is the carrier power to noise spectral density ratio for the residual carrier.
5. $\frac{P_{tone}}{N_0}$: This is the tone power (first harmonic only) to noise spectral density ratio.
6. $\frac{P_t}{N_0}$: This is the total signal power to noise spectral density ratio.

For carrier detection, define:

$$M = T\Delta f$$

$$f_s(x) = I_{M-1}\left(\sqrt{4\cdot x\cdot T\cdot CNR}\right)e^{-(x+T\cdot CNR)}\left(\frac{x}{T\cdot CNR}\right)^{\frac{M-1}{2}} \tag{8}$$

$$F_n(x) = 1 - \frac{\Gamma(M,x)}{\Gamma(M)} \tag{9}$$

Here, $\Gamma(M)$is the Euler gamma function and $\Gamma(M,x)$ is the incomplete gamma function [1]. Hence, the probability of correct detection for the residual carrier, which is one minus the probability of error is:

$$P = \int_{x=0}^{x=+\infty} I_{M-1}\left(\sqrt{4\cdot x\cdot T\cdot CNR}\right)e^{-(x+T\cdot CNR)}\left(\frac{x}{T\cdot CNR}\right)^{\frac{M-1}{2}} \left[1-\frac{\Gamma(M,x)}{\Gamma(M)}\right]^{N_f-1} dx \tag{10}$$

The key input parameters are T, Δf, N_f, and CNR.

For the probability of correct detection in resolving tones, assuming we have already correctly detected the carrier:

1. N_f: This is now the number of tones and not the number of frequency and frequency rate bins as it had been in the residual carrier case.
2. Replace CNR by $\frac{P_{tone}}{N_0}$
3. Define $M = 2T\Delta f$.

The resulting expression for the probability of correct tone detection is:

$$P = \int_{x=0}^{x=+\infty} I_{M-1}\left(\sqrt{4\cdot x\cdot T\cdot \frac{P_{tone}}{N_0}}\right)e^{-\left(x+T\cdot\frac{P_{tone}}{N_0}\right)}\left(\frac{x}{T\cdot\frac{P_{tone}}{N_0}}\right)^{\frac{M-1}{2}} \left[1-\frac{\Gamma(M,x)}{\Gamma(M)}\right]^{N_f-1} dx \tag{11}$$

MSL EDL

Significant events for the nominal parachute deploy case are shown in Table **1**. The 6DOF data was converted from Doppler frequency to sky frequency by adding MSL's downlink transmitted frequency (TFREQ) of 8,401,420,188.00 Hz and then a frequency offset of 9 KHz. The 6DOF data was originally in Spacecraft time (SCET), so one-way light time (OWLT) was added to obtain Earth Received Time (ERT).

Table 1- MSL EDL Critical Events 6DOF nominal parachute chute deploy case

ERT UTC	Time From Entry (s)	Meaning
	-3000.00	Switch to auxiliary oscillator (E- 50 min)
05:13:16	-677.00	Start of tones transmission with PLGA
05:13:42	-651.00	Calibration, carrier only
05:14:33	-600.00	Cruise Stage Separation
05:15:33	-540.00	Turn to Entry
	-484.86	eject cruise ballast mass -> center of mass offset
05:24:13	-20.00	Switch from PLGA to TLGA
		Entry Interface (radius 3522.2 km)
05:24:33	0	Flight Path Angle ~15.5 deg, +/- 0.05 deg
05:25:45	72.26	start of bank first reversal
05:25:45	72.39	maximum heating
05:25:52	79.30	maximum deceleration
05:25:57	83.88	end of first bank reversal
05:26:06	93.26	start of bank second reversal
05:26:17	103.51	end of second bank reversal
05:26:36	123.13	start of bank third reversal
05:26:46	133.01	end of third bank reversal
		Stand Up Fly Right -> zero center of mass offset
05:28:49	255.77	Parachute Deploy, carrier only
05:29:08	274.89	Heatshield Deploy
05:29:46	313.00	Loss of DTE communication
05:30:37	363.79	Backshell Separation, switch to DLGA
05:31:14	400.58	Rover Deploy
05:31:30	417.19	Touchdown, carrier only
05:31:31	417.80	Flyaway
		Descent Stage Impact

Residual frequency, frequency rate, and frequency acceleration were computed and the late chute case is shown in Figure 7, Figure 8, and Figure 9 respectively. Residual frequency changes slowly until Entry. As the spacecraft accelerates towards Mars, it banks three times. During banking, residual frequency rates reach +/- 300 Hz/s and residual frequency accelerations exceed +/- 100 Hz/s^2. After banking is complete, residual frequency changes

slowly until parachute deployment at E+255 seconds. As the time of parachute deployment is unknown, the navigation predicts do not contain this event, causing a large jump in residual frequency, rate, and acceleration.

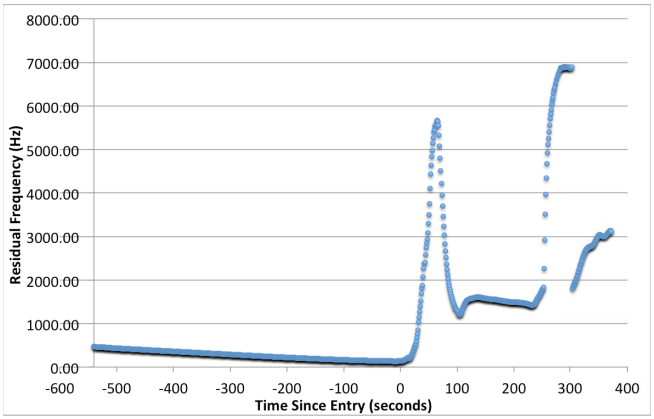

Figure 7- Residual Frequency for late chute case

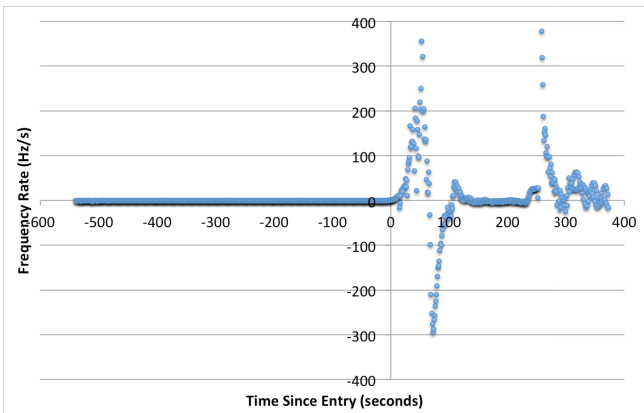

Figure 8- Residual Frequency Rate for late chute case

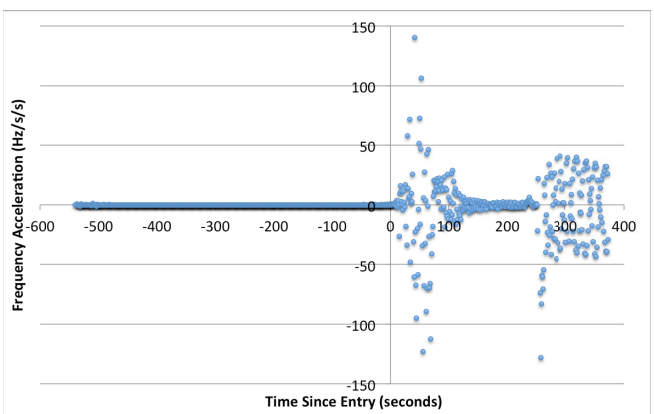

Figure 9- Residual Frequency Acceleration for late chute case

Total received signal power (carrier plus data)-to-noise spectral density ratio (P_t/N_o) was predicted to be greater than 20 dB-Hz from when the spacecraft started transmitting tones at E-677 seconds until loss of direct to Earth communications at E+313 seconds (due to the loss of a line of sight from Mars to Earth). This loss was a consequence of the geometry of the landing site and spacecraft trajectory. Predicted total received signal power to noise spectral ratio is shown in blue in Figure **10**. In this the late chute case, minimum P_t/N_o until loss of DTE communications at E+313 seconds is 28 dB-Hz. The off bore-sight/cone (theta) and clock (phi) angles of MSL's low gain antennas are plotted in green and red respectively.

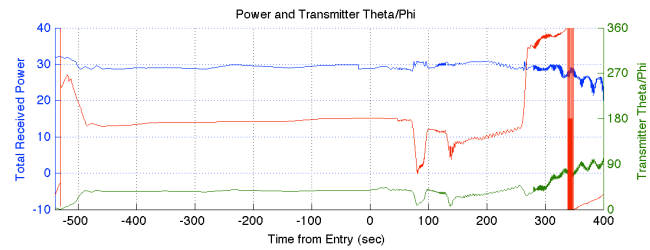

Figure 10- Predicted P_t/N_o for 6DOF late chute case

These signal characteristics were used to partition MSL EDL into three segments for processing by the EDA: Pre-Entry, Entry, and Parachute. Each segment used different configuration parameters.

Simulation Parameters

EDA software simulations utilized various parameters shown in Table **2**. These parameters describe properties of the MSL EDL tones design and were fixed for all simulations. A modulation index of 43° was chosen based on the need to maximize the probability of tracking the carrier and subcarrier [1]. Tones ranged in subcarrier frequency from 2 kHz to 20 kHz from the carrier. This design choice balanced the conflicting desires for smaller spacing between tones (and a smaller channel with less bandwidth streamed in real-time) and larger spacing between tones (increasing the probability of adjacent tones being correctly detected). Tone duration was 10 seconds. Simulations of detection probabilities performed for Mars Exploration Rover (MER) demonstrated that 10-second tones with P_t/N_o > 20 dB-Hz could be correctly detected >99% of the time [3]. Mars Science Laboratory requirements were for 90% correct detection.

A 100 kHz channel was used for recording. This channel's bandwidth of +/- 50 kHz is large enough to contain the complete range of tones (+/- 20 kHz), as well as expected changes in residual Doppler frequency due to uncertainties in predicts (+/- 8 kHz) and auxiliary oscillator drift with temperature (+/- 20 kHz). Maximum Doppler residual frequency change due to predicts was determined by differencing the bounding chute cases with the predicts. The auxiliary oscillator was expected to increase from -3°C to 11°C in the worst case. This temperature change causes frequency drift. To estimate this drift, models based on SDST laboratory test results were used.

Table 2- Key EDA simulation parameters

Parameter Definition	Parameter Name	Value
Length of simulation	LENGTH	15 minutes, 5 seconds
Sampling rate	SAMPLE_RATE	100 kHz
Modulation index (Δ)	MOD_INDEX	43°
Number of tones	TON_NUMBER	256
Frequency offset where tones begin	TON_OFFSET	2000 Hz
Frequency delta between tones	TON_DELTA	70.5883 Hz
Tone duration	TONE_DWELL	10 seconds

For the EDA software simulations, Radio Science Receiver data files were generated including a signal with the parameters specified in Table **2**. The simulation time ranged from E-540 seconds (when the 6DOF data started) to E+365 seconds (52 seconds after expected occultation). The frequency residual data from the 6DOF late chute data shown in Figure **7** was used. 10-second duration tones were also added. The EDA software calculates the subcarrier frequency of tone number n as shown below in Equation 1. For MSL, the EDA software calculates the subcarrier frequency of tone number n using a spacing of 70.5883 Hz between tones as shown in Equation 2. However, the MSL SDST uses Data Numbers (DNs) that must be integer numbers to specify sub-carrier frequency values. The actual tone spacing implemented by MSL varied between 66 DN = 70.81 Hz and 65 DN = 69.74 Hz. Actual tone spacing varied less than 1 Hz from the tone spacing used by the EDA software. The EDA was configured to allow for this difference.

$$f_{tone} = \text{TON_OFFSET} + n*\text{TON_DELTA} \quad (12)$$

$$f_{tone} = 2000 + n*70.5883 \text{ Hz} \quad (13)$$

Total power to noise ratio (P_t/N_o) is a configurable parameter and was varied from 30 dB-Hz down to 20 dB-Hz for different test runs.

EDA Configuration

The EDA utilizes a configuration file that specifies parameters to use for processing. An activity such as MSL EDL can be broken up into different configuration segments with start/stop times. Each configuration segment may utilize different signal processing parameters. The configuration segments used in MSL EDL are shown in Table **3**. In 6DOF simulations, the earliest time that parachute deployment occurred was at E+231 seconds; the parachute configuration segment started 10 seconds before this time for additional margin.

Table 3- MSL EDA Configuration Segments

Segment	Start time	End time
Pre-Entry	E-540	E-100
Entry	E-99	E+220
Parachute	E+221	E+365

Let $\dot{f}_{max}$ be the maximum residual frequency rate and $\ddot{f}_{max}$ be the maximum residual frequency acceleration.

A rule of thumb for FFT resolution is that the maximum frequency change during the interval in which the FFT is computed < Δf/4 [3].

$$\Delta f > \sqrt{4\,\dot{f}_{max}} \quad (14)$$

Using $\dot{f}_{max}$ of 400 Hz/s from Figure **8** yields Δf > 40 Hz. Based on this calculation, an FFT resolution of 40 Hz was chosen for the parachute configuration segment.

A rule of thumb for time of incoherent integration is that it be sufficiently short that the maximum deviation of the received carrier frequency from a linear trajectory over the T-length segment is < Δf/4 [3].

$$T < \sqrt{2\,\frac{\Delta f}{\ddot{f}_{max}}} \quad (15)$$

Using Δf = 40 Hz and $\ddot{f}_{max}$ of 150 Hz/s/s from Figure **9** yields T < 0.73 seconds. The minimum time of incoherent integration for the EDA is 1 second, so the system was configured with a value of T = 1 second. This decision implied that some tones would be missed during periods of very high dynamics, such parachute deployment.

Key EDA configuration parameters for the pre-entry, entry, and parachute EDA configuration segments are shown in Table **4**, Table **5**, and Table **6** respectively.

Table 4- Key EDA configuration parameters for Pre-Entry segment

Parameter	**Acquisition State**	**Tracking State**
FFT resolution (Δf)	2 Hz	2 Hz
Number of samples/FFT (N_{FFT})	50,000	50,000
Time of coherent integration (τ)	0.5 seconds	0.5 seconds
Time of incoherent integration (T)	1 second	1 second
Number of averaged FFTs (M)	2	2
Carrier frequencies to search	Entire 100 kHz channel	+/- 100 Hz
Subcarrier frequencies to search	+/- 2 Hz	+/- 2 Hz
Pre-FFT frequency rate search	+/- 35 Hz/s	+/-14 Hz/s
Number of Pre-FFT frequency rate bins (N_r)	15	15
Post-FFT frequency rate search	+/- 2 Hz/s	+/- 1 Hz/s
Threshold SNR	15.5 dB	14.5 dB
Search space (N_f)	750,000	750,000

Table 5- Key EDA configuration parameters for Entry segment

Parameter	**Acquisition State**	**Tracking State 1**	**Tracking State 2**
FFT resolution (Δf)	10 Hz	5 Hz	5 Hz
Number of samples/FFT (N_{FFT})	10,000	20,000	20,000
Time of coherent integration (τ)	0.1 seconds	0.2 seconds	0.2 seconds
Time of incoherent integration (T)	1 second	1 second	1 second
Number of averaged FFTs (M)	10	5	5
Carrier frequencies to search	Entire 100 kHz channel	+/- 200 Hz	+/- 200 Hz
Subcarrier frequencies to search	+/- 10 Hz	+/- 5 Hz	+/- 5 Hz
Pre-FFT frequency rate search	+/- 1400 Hz/s	+/-35 Hz/s	+/- 21 Hz/s
Number of Pre-FFT frequency rate bins (N_r)	15	15	15
Post-FFT frequency rate search	+/- 100 Hz/s	+/- 4 Hz/s	+/- 2 Hz/s
Threshold SNR	14.0 dB	13.5 dB	12.5 dB
Measure and feedback accelerations to tracking loop	off	off	on
Search space (N_f)	150,000	300,000	300,000

Table 6- Key EDA configuration parameters for Parachute segment

Parameter	Acquisition State	Tracking State
FFT resolution (Δf)	40 Hz	40 Hz
Number of samples/FFT (N_{FFT})	2,500	2,500
Time of coherent integration (τ)	0.025 seconds	0.025 seconds
Time of incoherent integration (T)	1 second	1 second
Number of averaged FFTs (M)	40	40
Carrier frequencies to search	Entire 100 kHz channel	+/- 600 Hz
Subcarrier frequencies to search	+/- 10 Hz	+/- 5 Hz
Pre-FFT frequency rate search	+/- 500 Hz/s	+/-350 Hz/s
Number of Pre-FFT frequency rate bins (N_r)	21	15
Post-FFT frequency rate search	+/- 140 Hz/s	+/- 125 Hz/s
Threshold SNR	10.0 dB	7.0 dB
Search space (N_f)	52,500	37,500

Theoretical probabilities of carrier and tone detection, *P*, were computed based on similar work for MER [7] and using the equations described in [1]. The parameters shown in Table **4**, Table **5**, and Table **6** were used. The probability of missed carrier acquisition ($1-P_{aq}$) vs P_t/N_o is shown for the parachute segment tracking state in Figure **11**. For a desired probability of carrier acquisition of 99.9%, the threshold P_t/N_o is about 23 dB-Hz. The probability of missed tone acquisition ($1-P_{aq}$) vs P_t/N_o is shown for the parachute segment tracking state in Figure **11**. For a desired probability of carrier acquisition of 99.9%, the threshold P_t/N_o is about 21 dB-Hz.

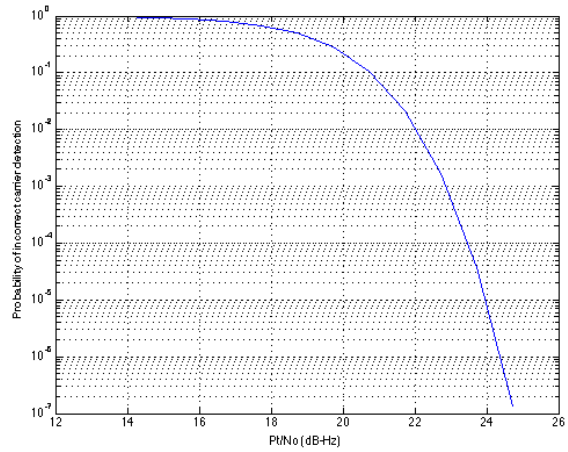

Figure 11- Probability of missed carrier acquisition for parachute segment acquisition state

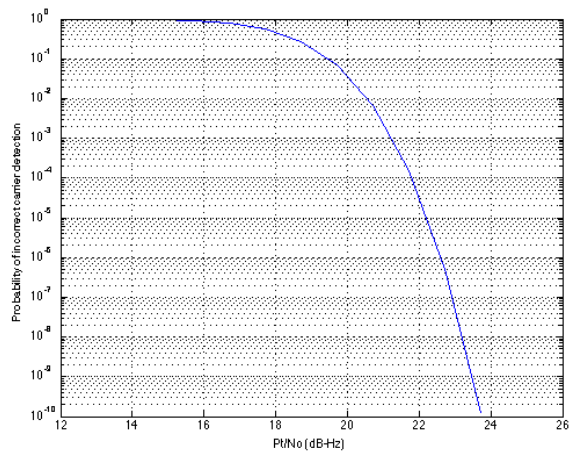

Figure 12- Probability of missed tone detection for parachute segment state

Using the configuration parameters specified in Table **6** for the parachute segment state, tone detection is harder than carrier detection. Predicted minimum P_t/N_o was 28 dB-Hz (as shown in Figure **10**), so there were several dB of margin for both carrier acquisition/tracking and tone detection. The parachute segment was the most challenging, due to two factors: a) higher dynamics, including a discontinuity in residual frequency during parachute deployment and b) lower predicted P_t/N_o due to swinging on the bridle and associated TLGA angles.

4. RESULTS

DSS-43 70-m Data

MSL Entry, Descent, and landing took place on August 5, 2012 UTC. Key tones are shown in Table **7**, along with the expected and actual times of receipt on Earth. Expected times are from the nominal chute case. The bank 1 tone occurred about 2 seconds later than the nominal 6DOF run and the bank angle was between 45° and 90° as expected. The bank 2 tone occurred about 6 seconds later than the nominal time and the bank angle was between -90° and -45° as expected. The bank 3 tone occurred about 2 seconds earlier than the nominal time and the bank angle was between 45° and 90° as expected. The maximum deceleration tone was received about 9 seconds later than the nominal time and maximum deceleration was between 11 and 12 Gs.

Table 7- Key MSL EDL Tones

Event	**Expected Time from Entry (seconds)**	**Actual Received Time from Entry (seconds)**
Tone start	E-677	E-658
Cruise stage separation	E-600	E-600
Switch from PLGA to TLGA	E-20	E-20
Entry	0	0
Start of bank 1	E+72.26	E+74
End of bank 1	E+83.88	E+85
Maximum deceleration	E+79.30	E+88
Start of bank 2	E+93.26	E+99
End of bank 2	E+103.51	E+110
Start of bank 3	E+123.13	E+121
End of bank 3	E+133.01	E+132
Stand-Up-Fly-Right	E+239	E+240
Parachute Deploy	E+255.77	E+260
Heat shield Deploy	E+274.89	E+283
Loss of DTE communication	E+313	E+299

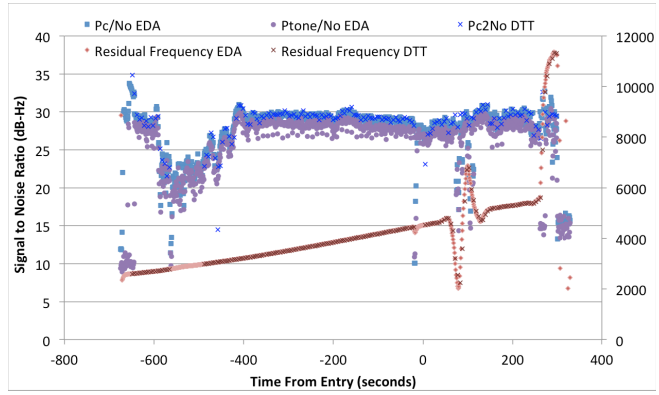

Figure 13- MSL EDL P_c/N_o, P_{tone}/N_o, and Residual Frequency with DSS-43

Direct-to-Earth data received at DSS-43 during MSL EDL is shown in Figure **13**. Carrier-to-noise power (P_c/N_o) (plotted in light blue) measured by the EDA matched closely with P_c/N_o measured by the closed-loop receiver (dark blue). Average P_c/N_o measured by the EDA using DSS-43 during EDL was 27.8 dB-Hz, consistent with predictions made by the MSL Telecommunications team [5]. Average tone power to noise spectral density ratio (P_{tone}/N_o) (plotted in purple) was 26.4 dB-Hz. Cruise stage separation (CSS) caused a 7 second signal outage as the Parachute Low Gain Antenna (PLGA) was briefly obstructed. The antenna swap from PLGA to Tilted Low Gain Antenna (TLGA) resulted in a 4 second signal outage.

Residual frequency as measured by the EDA (plotted in light red) and the closed loop receiver (dark red) matched closely as shown in Figure **13**. The closed-loop receiver lost lock at the following times: Cruise Stage Separation, PLGA-to-TLGA swap, banking, and parachute deployment. The changes in frequency observed during EDL can be attributed to two factors: 1. Doppler induced by events during EDL such as atmospheric entry, cruise stage separation, and parachute deployment; and 2. Changes in the output frequency of the auxiliary oscillator (AUX OSC) in the Small Deep Space Transponder (SDST), which are chiefly due to changes in temperature.

Entry was predicted for 5:24:33 UTC in the navigation predicts file and actually occurred 1 second later, at 5:24:34 UTC. This difference between predicted and actual entry time and banking times resulted in the Doppler shift of about 4 kHz between E+50 seconds and E+150 seconds. The navigation predicts file also did not include parachute deployment, resulting in a large jump in residual frequency at around E+260 seconds.

Figure **14** illustrates frequency as a function of AUX OSC and Baseplate temperature. Cubic polynomials provide a good approximation to the frequency versus temperature behavior of the SDST AUX OSC crystal, particularly in this temperature region. The R^2 value for the AUX OSC

temperature sensor polynomial is 0.9977, while the R^2 value for the baseplate temperature sensor polynomial is 0.9984. Table **8** presents the polynomial coefficients.

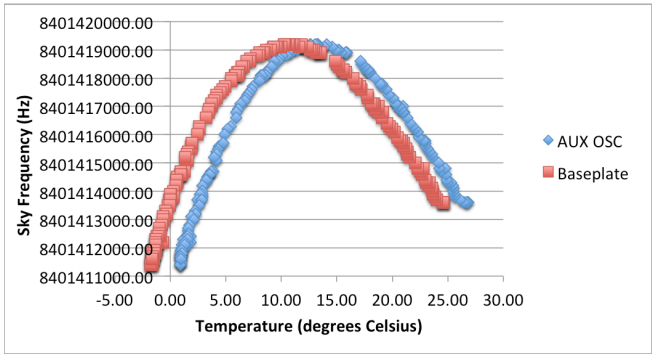

Figure 14- Frequency (Hz) vs Temperature (degrees Celsius) for Auxiliary Oscillator and Baseplate

Table 8- Coefficients for Frequency vs Temperature Polynomials

Coeff	x^3	x^2	x^1	1
AUX OSC Sensor	0.782246404	-72.49066315	1489.915415	8401410276
Baseplate Sensor	0.824981981	-66.82276803	1134.968993	8401413648

Although the high R^2 values seem to provide reason for confidence in these temperature predictions, the EDL thermal environment differs notably from that in cruise. Steady temperatures and thermal equilibrium characterize the cruise thermal environment. The EDL thermal environment is characterized by rapid heating. As a result, the SDST and its internal components were not in thermal equilibrium during EDL. In thermal equilibrium, as shown in Figure **15** below, the AUX OSC is normally somewhat warmer than the baseplate. However, as Figure **15** also shows, during EDL, the baseplate temperature rose relatively quickly and rapidly overshot the AUX OSC temperature. Although AUX OSC temperature rose slowly to "catch up" with baseplate temperature, the SDST was not in thermal equilibrium during EDL. This impacts the accuracy of any frequency predictions based on baseplate temperature.

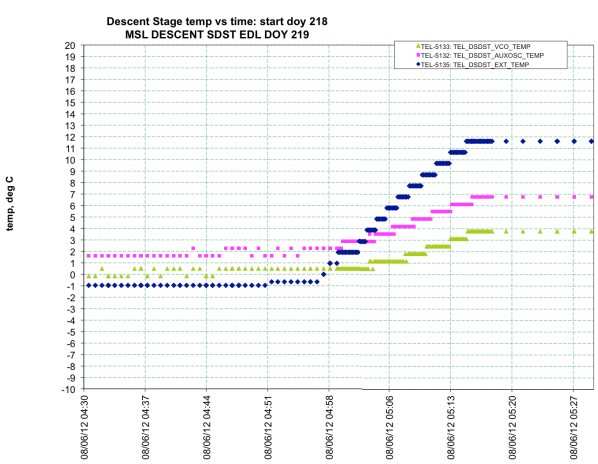

Figure 15- MSL EDL SDST Temperatures

DSS-34/DSS-45 34-m Array Data

As a backup to the prime 70-m antenna (DSS-43), the signals from a beam waveguide 34-m antennas (DSS-34) and a high efficiency 34-m antenna (DSS-45) were combined and recorded. This back-up data was not needed in real-time and was analyzed in post-processing.

Direct-to-Earth data received by the DSS-34/DSS-45 array during MSL EDL is shown in Figure **16**. Average carrier-to-noise power (P_c/N_o) (plotted in light blue) measured by the EDA using the DSS-34/DSS-45 array during EDL was 23.5 dB-Hz.

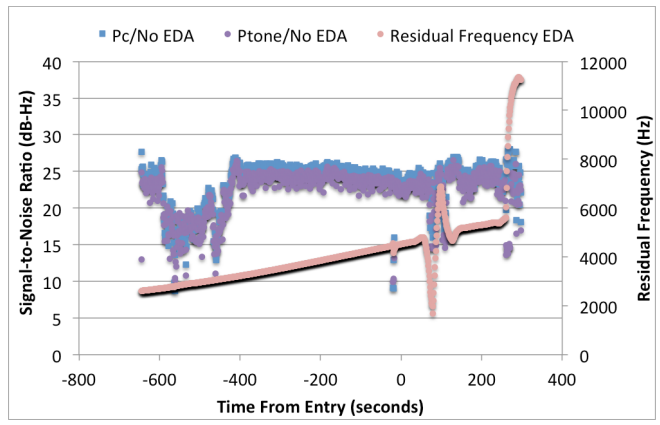

Figure 16- MSL EDL P_c/N_o, P_{tone}/N_o, and Residual Frequency with DSS-34/DSS-45 Array

Antenna sensitivity is measured by *G/T*, where *G* is the antenna gain, and *T* is the system noise temperature. *G* is a function of wavelength, λ, physical aperture area, A_p, and aperture efficiency, η, as shown below.

$$G = \frac{4\pi}{\lambda^2} A_p \eta \tag{16}$$

Based solely on physical aperture area, A_p, the *G/T* of a 34-m antenna is about (17.0*17.0)/(35.0*35.0) = 23.6% the *G/T* of a 70-m antenna. However, the DSN 70-m antenna also has better aperture efficiency, η, and a lower system noise temperature, *T*, than the DSN 34-m antennas. With these factors considered, the *G/T* of a DSN 34-m antenna is about 18% the *G/T* of a DSN 70-m antenna [8]. The predicted difference in array gain between the 70-m antenna and two arrayed 34-m antennas is $10*\log_{10}(1.0/(.18+.18))$ = 4.44 dB, assuming no combining loss. P_c/N_o is proportional to *G/T*. The measured difference in P_c/N_o during EDL between DSS-43 and DSS-34/DSS-45 is shown Figure **17**. The mean measured difference from E-645 seconds to E+299 seconds was 4.26 dB. Therefore mean combining loss during this time was about 0.18 dB.

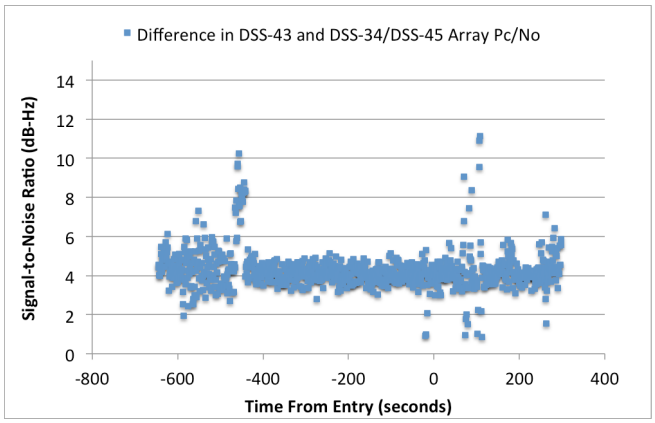

Figure 17- Difference in DSS-43 and DSS-34/DSS-45 P_c/N_o

After EDL, Event Records (EVRs) that logged each tone issued during EDL were obtained from MSL. These logs were compared with the real-time results provided by the EDA to determine performance. The DTE communications system received and correctly identified 100% of radiated tones in real-time during MSL EDL. These results are consistent with the theoretical probabilities of carrier acquisition/tracking and data tone detection computed in Section 3.

5. CONCLUSION

The Direct-to-Earth X-band communications system utilized during MSL EDL successfully detected all radiated tones, despite challenging signal dynamics with large unknown changes in Doppler frequency, rate, and acceleration. Future missions with periods of rapid and unknown signal dynamics such as Mars or icy moon landers can leverage from the MSL design for DTE communications.

6. ACKNOWLEDGEMENTS

The authors would like to acknowledge the contributions of Jan Tarsala in the testing of the EDA prior to MSL EDL using a PRSR and MSL testbed. The authors would like to thank Jeremy Shidner for providing 6DOF simulation data that was valuable in configuring the EDA. The authors would also like to thank the CDSCC station personnel for their excellent support and operations of the DSN equipment and the Full Spectrum Processor Array in particular.

This research was carried out at the Jet Propulsion Laboratory, California Institute of Technology. Copyright 2012 California Institute of Technology. Government sponsorship acknowledged.

REFERENCES

[1] E. Satorius, P. Estabrook, J. Wilson, D. Fort. "Direct-to-Earth communications and signal processing for Mars exploration rover entry, descent and landing," The Interplanetary Network Progress Report, IPN Progress Report 42-153, May 2003.

[2] Andre Jongeling and Susan Finley. "Mars Science Laboratory Telecom System Engineering Pre-CDR Peer Review: EDL Data Analysis Simulations Results." April 24, 2007.

[3] W. J. Hurd, P. Estabrook, C. S. Racho, and E. Satorius. "Critical spacecraft-to-earth communications for Mars exploration rover (MER) entry, descent and landing," Proc. IEEE Aerospace Conference, vol.3, pp. 1283-1292, MT, March 2002.

[4] M. Soriano, S. Finley, A. Jongeling, D. Fort, C. Goodhart, D. Rogstad, R. Navarro, "Spacecraft-to-Earth Communications for Juno and Mars Science Laboratory Critical Events," Proc. IEEE Aerospace Conference, MT, March 2012.

[5] A. Makovsky, P. Illott, J. Taylor. "Mars Science Laboratory Telecommunications System Design," Deep Space Communications and Navigation Systems Center of Excellence Design and Performance Summary Series, November 2009.

[6] M. Soriano and P. Estabrook, "MSL EDL Simulations" (internal document), Jet Propulsion Laboratory, Pasadena, CA, May 7, 2012.

[7] E. Satorius, "Revised Thresholds for EDL" (internal document), Jet Propulsion Laboratory, Pasadena, CA, January 14, 2003.

[8] A. Kwok. "Module 206, Telemetry General Information." in *DSN Telecommunications Link Design Handbook*. Rev. B. DSN No. 810-005. Pasadena California: JPL, October 31, 2009. http://eis.jpl.nasa.gov/deepspace/dsndocs/810-005/

Melissa Soriano *is a staff software engineer in the Tracking Systems and Applications Section at the Jet Propulsion Laboratory. She has developed real-time software for Direct-To-Earth communications with Mars Science Laboratory during Entry, Descent, and Landing, the Long Wavelength Array, NASA's Breadboard Array, and the Wideband VLBI Science Receiver used in the Deep Space Network. Melissa is also currently the software cognizant engineer for the DSCC Downlink Array. She has a B.S. from Caltech, double major in Electrical and Computer Engineering and Business Economics and Management. She also has an M.S. in Computer Science from George Mason University.*

Susan Finley *is a key staff member in the Processor Systems Development Group at JPL. She is the subsystem engineer for the Full Spectrum Processor subsystem deployed in NASA's Deep Space Network. Her experience includes the operation of the EDA for both of the MER landings on Mars as well as the operation of the Radio Science Receiver for the landing of the Huygens Probe on Titan and for the Phoenix landing on Mars.*

David Fort *received a B.A.Sc.in Engineering Physics and M.Sc.in Astronomy from the University of Toronto and an M.Sc. and Ph.D. in Radio Astronomy from the University of Manchester. He joined NRC (Canada) in 1972 and worked on all aspects of VLBI until 1987. He subsequently joined JPL in section 335 and worked on a number of hardware and software projects for the DSN and became supervisor of the Processor Systems development Group for the two years prior to returning to NRC in 2002. Until his retirement in 2010 he worked on the EVLA Correlator Project. Now a "Guest Worker", he helps out with the EVLA as it becomes fully operational and with occasional questions from JPL.*

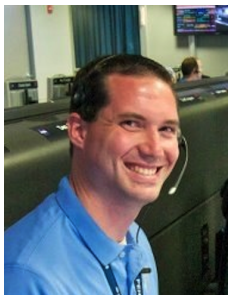

Brian Schratz *is the lead engineer for the EDL telecommunications on the Mars Science Laboratory mission and a member of JPL's Communications Systems and Operations group. He joined JPL three years ago with a B.S.E.E. and M.S.E.E. from The Pennsylvania State University.*

Peter Ilott *is the telecommunications system lead for the MSL mission. He has worked on spacecraft telecommunications system design for 25 years, 11 years on commercial spacecraft, and since 2000 at JPL. He worked on MER, Phoenix, as a telecommunications system engineer. Peter worked on all the Mars EDL (entry descent and landing) efforts since MER, and in between Mars missions helped out on the Deep Impact and Cloudat missions at JPL. He currently supports the MSL surface mission phase, and is the telecommunications lead for the Europa mission currently under study. Ilott holds BSc, MSc, and PhD degrees in physics and electrical engineering from McGill and the Univeristy of Montreal.*

Ryan Mukai *received the B.S.E.E. and the M.S.E.E. in 1997 and the Ph.D. in Electrical Engineering in 2003, all from UCLA. He has been employed at the Jet Propulsion Laboratory as a Telecommunications engineer since 1999 and has served on the Mars Exploration Rover, DAWN, Cassini, Juno, and Mars Science Laboratory projects.*

Polly Estabrook *is the deputy manager of the Communication Architectures and Research Section at JPL. She is a member of NASA's Space Communication and Navigation Program supporting the definition of the NASA's future Integrated Communication and Navigation Network and is a member of the Integrated System Engineering team for the Mars Science Laboratory rover. From 2005 to 2010, she led several communication system design teams with the goal of defining the modifications to NASA's Space Communication and Navigation infrastructure needed to support the planned human missions to the Moon and Mars. From 2000 to 2004 she was the lead telecom system engineer for the Mars Exploration Project, responsible for the performance of the entry descent and landing telecommunications system and for the overall design and performance of the Direct to Earth and relay communications systems. In 2004, Dr. Estabrook received the NASA Exceptional Achievement Medal for her work on the Mars Exploration Rover Telecom System. She has written over 35 technical papers and chaired numerous IEEE and AIAA conference Sessions. Polly Estabrook received her B.A. in engineering physics from the University of California, Berkeley, and M.S. and Ph.D. degrees in electrical engineering from Stanford University, Stanford, CA.*

Kamal Oudrhiri *is a senior member in the Radio Science Systems Group at NASA's Jet Propulsion Laboratory. As a contract technical manager, Oudrhiri led multi-disciplinary teams through the design, implementation and delivery of flight hardware to the radio science community. Over the last decade, Oudrhiri served in key roles on multiple NASA missions: The Mars Exploration Rovers (MER), the International Cassini mission to Saturn,The GRAIL lunar mission and The Mars Science Laboratory (MSL).*

Daniel Kahan *is a senior member of the Radio Science Systems Group at NASA's Jet Propulsion Laboratory. Over the last eight years, he has provided engineering support for the radio science community on multiple NASA missions, including Mars Global Surveyor, Mars Reconnaissance Orbiter, the GRAIL lunar mission, the International Cassini mission to Saturn, and Mars Science Laboratory.*

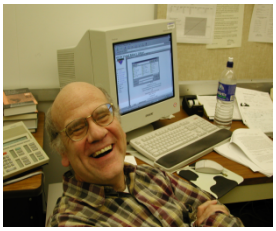

Edgar H. Satorius *is a principal member of the technical staff in the Flight Communications Systems Section of the Jet Propulsion Lab. He performs systems analysis in the development of digital signal processing and communications systems with specific applications to blind demodulation, digital direction finding and digital receivers. He has published over 90 articles and holds two patents in the field of digital signal processing and its applications. In addition, he is an Adjunct Associate Professor at the University of Southern California where he teaches digital signal processing courses. He received his B.Sc. in engineering from the University of California, Los Angeles and the M.S. and Ph.D. degrees in electrical engineering from the California Institute of Technology, Pasadena, California.*